

A COMPARISON OF DIRECT AND INDIRECT MASS ESTIMATES FOR DISTANT CLUSTERS OF GALAXIES*

Ian Smail^{1†}, Richard S. Ellis², Alan Dressler¹, Warrick J. Couch³,
Augustus Oemler Jr.^{4‡}, Ray M. Sharples⁵ & Harvey Butcher⁶,

- 1) The Observatories of the Carnegie Institution of Washington,
813 Santa Barbara St., Pasadena, CA 91101-1292
- 2) Institute of Astronomy, Madingley Rd, Cambridge CB3 0HA, UK
- 3) School of Physics, University of New South Wales, Sydney 2052, Australia
- 4) Astronomy Department, Yale University, PO Box 208101, New Haven CT 06520-8101
- 5) Department of Physics, University of Durham, South Rd, Durham DH1 3LE, UK
- 6) NFRA, PO Box 2, NL-7990, AA Dwingeloo, The Netherlands

Received —; accepted —

* Based on observations obtained with the NASA/ESA Hubble Space Telescope which is operated by STSCI for the Association of Universities for Research in Astronomy, Inc., under NASA contract NAS5-26555.

†Current address: Department of Physics, University of Durham, South Rd, Durham DH1 3LE, UK

‡Current address: The Observatories of the Carnegie Institution of Washington, 813 Santa Barbara St., Pasadena, CA 91101-1292

ABSTRACT

We present weak lensing results for 12 distant clusters determined from images obtained with the refurbished *Hubble Space Telescope*. We detect the signature of gravitational lensing in 11 of the 12 clusters; the clusters span nearly an order of magnitude in lensing strength. The sample thus provides an excellent database for correlating direct mass estimates based on lensing with indirect ones which rely on baryonic tracers. We examine the correlation between the cluster X-ray luminosities and the mean gravitational shear strengths and develop a model which allows us to predict the relationship expected from the properties of local clusters. After allowing for various observational effects, we find that the predicted correlation is a reasonable match to the available data, indicating that there has been little evolution in the X-ray luminosity–central mass relationship between $z \sim 0.4$ and now. We discuss the implications of this result in the context of the evolution of the X-ray luminosity function found by earlier workers. The comparison between shear amplitudes and velocity dispersions, estimated from a modest sample of members (~ 30), reveals a discrepancy in the sense that these velocity dispersions are typically over-estimated by factors of $\sim 50\%$. This supports earlier suggestions that high dispersions measured for distant clusters may be seriously affected by both unidentified substructure and outliers. Combining our shear-based mass estimates with morphologically-based luminosity estimates, we determine mass/light ratios of $M/L_V^{all} = 180_{-110}^{+210} h$ (M/L) $_{\odot}$ for the entire population and $620_{-240}^{+250} h$ for spheroidal population where the evolutionary effects can be best treated. We argue that this provides an upper bound to the present-day cluster mass/light ratio corresponding to $\Omega \sim 0.4$. Our results demonstrate the important role weak gravitational lensing can play in the study of the evolution of distant clusters, as the most direct and least biased probe of their growth.

Subject headings: cosmology: observations – gravitational lensing – clusters of galaxies: evolution

1. Introduction

Rich clusters of galaxies can be identified to high redshift and can thus be used as tracers of the evolution of structure. Moreover, as clusters represent the extreme tail of the fluctuation spectrum they provide a particularly sensitive probe of the form of the primordial power spectrum.

The most widely used techniques for identifying distant clusters are based on searches either for an overdensity in the projected galaxy distribution (Gunn, Hoessel & Oke 1986; Couch et al. 1991; Postman et al. 1996) or the detection of X-ray emission from hot gas bound to the cluster potential (Edge et al. 1990; Henry et al. 1992; Bower et al. 1994; Castander et al. 1995). However, the relatively high abundance of distant optically-selected clusters to $z \simeq 0.5$ appears to contradict the X-ray survey results which suggest a marked decline in the volume density of luminous X-ray systems beyond $z \simeq 0.2$. This conflict has led to the suggestion (Kaiser 1991) that the evolution of the X-ray luminosities of distant clusters need not simply reflect changes in the underlying potential wells. By including a minimum entropy in the gas prior to it entering the cluster, Kaiser was able to limit the compression the gas undergoes during the cluster formation, significantly altering the X-ray evolution. If confirmed, this would seriously complicate the use of X-ray observations for studying the evolution of the mass function of distant clusters. It would also raise interesting issues for the growth of structure in the universe and the thermal evolution of the hot X-ray gas in clusters (Kaiser 1991; Castander et al. 1995; Bower 1996).

The optical richness of a cluster is clearly more prone to projection effects than the cluster’s X-ray luminosity. To try to reduce this problem, a number of groups are undertaking spectroscopic surveys of distant clusters to provide membership information, in addition to estimating the cluster velocity dispersions. However, rather than using indirect baryonic tracers such as cluster galaxies or hot X-ray gas, it would clearly be preferable to consider more direct measures of the cluster mass. The most direct measure comes from the analysis of the weak gravitational lensing signal detected using the shapes of field galaxies seen through the cluster. The lensing method can provide an absolute measure of the cluster mass and can be readily applied to intermediate and distant rich clusters. At the same time it is insensitive to the thermodynamical state of the baryonic components in the cluster, a particularly important advantage when considering clusters at high redshift which may not be fully virialised.

We report in this paper on a study of the lensing properties of 12 distant clusters which have been imaged using the *Hubble Space Telescope* (HST). The clusters span a wide range in redshift ($z = 0.18\text{--}0.58$), X-ray luminosity and optical richness, and thus comprise an ideal sample for investigating the relative evolution of the mass, X-ray and galaxian properties of distant clusters. The key to our study is the derivation of mass estimates from the cluster’s lensing effect on uniformly-selected samples of background

faint field galaxies. By measuring the distortion of this population we obtain a robust measure of the mass in the central regions of the foreground clusters. Using simple, empirical models of the clusters, we then compare the predicted X-ray luminosities and velocity dispersions, calculated from our mass estimates and local scaling relations, with the observed quantities to distinguish between models for the evolution of the cluster properties. We then proceed to use our lensing mass estimates, along with morphologically classified samples of cluster galaxies, to estimate the mass to light ratios of our clusters.

A plan of the paper follows. The cluster dataset and its reduction is summarized in §2 and the lensing analysis and modelling described in §3. We discuss the results and compare the various mass estimates in §4, where we also give the mass to light ratios (M/L) estimated from our lensing analysis before summarizing our conclusions in §5.

2. Data

The bulk of the HST data used for this study were obtained as part of a Cycle-4 WFPC-2 program to investigate the morphological evolution of cluster galaxies. This sample comprises ten distant clusters which have been the subject of an intensive ground-based campaign by ourselves and other groups over the past decade. Data for two other clusters (Cl0440–02 and Cl0024+16) have been retrieved from the HST archive. The full dataset does not constitute a “complete” sample in any respect, but is ideally suited for our purpose since they span a wide range of optical richness and X-ray luminosity and have been well-studied hitherto. As we show below, the wide range in properties is essential to adequately test for differential evolution between the various estimators of the cluster mass. The important issue for our analysis is the fact that these HST images are sufficiently deep to provide reliable information on the weak lensing of background galaxies viewed through the clusters.

The cluster sample, together with relevant observational details, is given in Table 1. The filters used for the observations discussed here are F555W (V_{555}), F702W (R_{702}) and F814W (I_{814}). The individual exposures were generally grouped in sets of 4 single-orbit exposures each offset by 2.0 arcsec to allow for hot pixel rejection. After standard pipeline reduction, the images were aligned using integer pixel shifts and combined into final frames using the IRAF/STSDAS task CRREJ. We retain the WFPC-2 color system and hence use the zero points from Holtzman et al. (1995). The final images cover the central $0.4\text{--}0.8\text{ h}^{-1}\text{ Mpc}^{\S}$ of the clusters (Fig. 1) to a 5σ limiting depth of $I_{814} \simeq 26.0$ or $R_{702} \simeq 26.5\text{--}27.0$. In the following analysis

[§]We use $q_o = 0.5$ and $h = H_o/100\text{ km sec}^{-1}\text{ Mpc}^{-1}$. This geometry means that 1 arcsec is equivalent to $1.88\text{ h}^{-1}\text{ kpc}$ for our lowest redshift cluster and $3.76\text{ h}^{-1}\text{ kpc}$ in the most distant.

we use the reddest band available for a particular cluster to identify objects and measure their shapes. The V_{555} images are used primarily for determining colors, which aid in identifying cluster members.

To catalog faint objects in these frames and measure their shapes we used the SExtractor image analysis package (Bertin & Arnouts 1996). We adopt a detection isophote equivalent to $\sim 1.3\sigma$ above the sky, where σ is the standard deviation the sky noise, viz. $\mu_{814} = 25.0$ mag arcsec $^{-2}$ or $\mu_{702} = 25.7$ mag arcsec $^{-2}$ ($\mu_{702} = 25.0$ mag arcsec $^{-2}$ for A2218, AC103 and AC118), and a minimum area after convolution with a 0.3 arcsec diameter top-hat filter of 0.12 arcsec 2 . Analysis of our exposures provides catalogs of ~ 800 objects for each cluster across the 3 WFC chips. We discard the smaller, lower sensitivity, PC fields as well as a narrow border around each WFC frame in the following analysis.

To compare the lensing strengths of the various clusters we must construct well-defined samples of background galaxies for which image parameters can be measured with adequate signal-to-noise. For simplicity in modelling we have adopted uniform magnitude limits across the sample. The faint magnitude limit is determined by the depth at which reliable images shapes can be measured in our shortest exposures. This is $R_{702} = 26.5$, as set by the A2218, AC103 and AC118 exposures. The bright limit is set by our desire to reduce cluster galaxy contamination in the field samples for the most distant clusters. Using colors, we can determine the point at which the color-magnitude relation for the cluster ellipticals blends into the background population. Fainter than this point the field population dominates (see below). This corresponds to a bright limit of $I_{814} = 24.0$. When converting between the R_{702} and I_{814} limited samples, we have assumed a typical color for the faint field population at these depths of $(R_{702} - I_{814}) \sim 0.5$ (Smail et al. 1995b).

Applying these limits yields a typical surface density of ~ 95 field galaxies per arcmin 2 , in good agreement with that measured in genuine ‘blank’ fields ($\sim 95 \pm 10$ arcmin $^{-2}$) after correcting for differences in the photometric systems (Smail et al. 1995b). We thus estimate that any residual contamination in our catalogs from faint cluster members must be less than ~ 5 –10%. The final sample size in a typical cluster, after applying both the magnitude and the area cuts (see below), is ~ 180 galaxies.

Additional cluster data is also given in Table 1. This includes rest-frame velocity dispersions from Couch & Sharples (1987), Dressler & Gunn (1992) and Le Borgne et al. (1992). These are estimated using standard procedures (Danese et al. 1980) using those authors’ own redshift catalogues without further corrections. We also give X-ray luminosities in the 0.3–3.5 keV band, taken from the literature (Castander et al. 1994; Henry et al. 1982; Wang & Stocke 1993), when available. For four of the clusters (AC118, Cl0939+47, Cl0412–65 and Cl0054–27) no published data were available and for these we measured luminosities from archival ROSAT PSPC images of the clusters. The cluster flux is measured inside an

optimal aperture, determined from the cluster’s detection significance, and then corrected to a total flux using a β -model with $\beta = 2/3$ and $r_c = 125 h^{-1}$ kpc. When required, we converted the X-ray luminosities to the 0.3-3.5 keV band assuming a mean cluster temperature of 7 keV; this is typically a correction of $\simeq 20\%$. We adopt a mean cluster temperature of 7 keV when calculating these corrections. No attempt has been made to remove emission arising from either a central cooling flow or any faint embedded point sources.

3. Analysis

3.1. Weak Lensing Measurements

We now discuss our methods for measuring the cluster shear from the catalogs of faint objects described above.

Two-dimensional shear maps have been constructed from the complex shear: $g = \epsilon e^{2i\phi}$, where ϕ is the position angle of the major axis of a faint image and $\epsilon = (a - b)/(a + b)$ is a shape estimator for an image of major and minor axes a and b (Kneib et al. 1995). This quantity is calculated for every image in the catalog and the shear estimates are binned into independent 20×20 arcsec cells and plotted as a vector field over the frame. A number of our clusters show strongly coherent shear fields (Fig. 1) which provide a very powerful and direct view of the cluster potential well including its center, ellipticity and orientation. In other cases the coherence of the shear field is more difficult to discern and we must assume symmetry, and in some cases a center for the shear field, before we can proceed with our analysis. In these cases, we assume, following clear trends observed with our stronger lenses, that the shear geometry is roughly circular and centered on the brightest cluster member.

The total shear strength of a cluster, $\langle g_1 \rangle$, was calculated using the average tangential shear ($g_1 = -\epsilon \cos(2\theta)$, where θ is the angle between the major axis and the vector joining it to the lens center) for all the images contained within an annulus $r = 60\text{--}200 h^{-1}$ kpc around the lens center. The shear is determined in annular sections between the two radii and corrections applied for any fraction of the annulus falling outside the WFC boundary. Errors are determined by bootstrap resampling of the data and are thus likely to be liberal estimates. The outer annulus represents the largest metric radius common to all the clusters which does not involve a large correction for areas off the frame. The inner radius has been chosen so as to reduce any underestimation of the shear in the central regions, due to either our adopted shear estimator or the difficulties in detecting faint lensed features against the halos of the luminous central cluster galaxies.

To determine the contribution to the observed shear from systematic effects in the HST optics,

detectors, or the reduction method, we have also applied our analysis to a similarly deep image of a blank field. This archival data consists of deep V_{555}/I_{814} WFPC-2 images of a blank field from the ‘‘Groth Strip’’. The data was processed and object catalogs generated in a similar manner as before. The mean tangential distortion using our standard annulus and magnitude limits was found to be $\langle g_1 \rangle = -0.008 \pm 0.070$. The quoted error represents the field-to-field scatter, which is similar to the uncertainty determined by boot-strap resampling.

One final step is required to place all our shear measurements on a comparative scale. Notwithstanding the uniform magnitude limits, the different redshifts of the various clusters means that each experiences a different proportion of foreground field contamination. Furthermore, because lensing depends on the relative distances of the lens and background source, even identical clusters at different redshifts will produce different shear effects on the same background population. We have therefore corrected all the observed shear signals to that appropriate for a putative cluster placed at the mean redshift of our sample, $\langle z \rangle \sim 0.4$, lensing a population of galaxies at $z \gg 0.4$.

To determine this correction we need to make the following assumption: that the background population viewed through all the clusters can be well described by a single redshift distribution, $N(z)$. Following the inversion analysis of the cluster A2218 by Kneib et al. (1995), we assume the no evolution form for our magnitude-limited sample, ignoring possible differences between the R_{702} and I_{814} selection. This $N(z)$ has a median $z = 0.83$ with only $\sim 10\%$ of the field population at $z < 0.4$. As the correction is differential we do not expect residual uncertainties arising from the assumed $N(z)$ to be significant.

3.2. Observational Factors

Here we calculate the effect of those observational factors which may degrade the amplitude of the observed shear signal. Such effects include possible inefficiencies in the image analysis algorithm, image crowding, low signal-to-noise in the image shapes and residual cluster contamination. Earlier workers have estimated the correction from observed to true shear to be around ~ 2 – 3 for ground-based observations (Kaiser, Squires & Broadhurst 1995; Wilson, Cole & Frenk 1996), where the majority of the degradation arises from atmospheric seeing. Working with HST we can thus expect a smaller correction.

To estimate our observational efficiency we have used two approaches. Firstly, we have taken HST images of deep blank fields and sheared them by known amounts, added in sky noise to simulate the depth of our cluster exposures and then re-measured the shear signal from these images. Secondly, we have created artificial images matched as closely as possible to the characteristics of our observations (e.g. magnitude and

scale size distributions of the field population, sky noise, etc.) and introduced a known amount of coherent shear. By applying our analysis technique we can then determine the efficiency of our shear measurement. From these experiments we determine a degradation of $\sim 0.8_{-0.2}^{+0.1}$.

Comparing the surface densities of faint galaxies in our fields to counts from blank fields, we estimate that the maximum contribution from faint cluster members will be less than $< 10\%$. Assuming that these faint images are randomly orientated, they will degrade the observed shear signal on average by $\sim 5\%$. Combining this with the estimated analysis efficiency we obtain a total efficiency of $\sim 0.75 \pm 0.20$. This signal degradation can now be included in our model predictions (see below) when comparing them to the observations.

3.3. Theoretical Predictions

Before comparing the cluster masses derived from our shear measurements with the X-ray luminosities (L_X) and cluster velocity dispersions (σ), we need to predict the expected behaviour of the L_X –shear and σ –shear correlations using simple models for the expected evolution of clusters. Although this is clearly a complex issue, our aim in this paper is to adopt a simpler approach, based on a number of elementary assumptions, seeing whether these are capable of reproducing the correlations observed in our sample.

We first examine the expected X-ray luminosity for a cluster lens as a function of its shear amplitude. To estimate an upper limit on the predicted shear for a given cluster mass, we consider the hardest cluster potential likely: nearly-singular isothermal spheres. Such potentials are supported by the mass profiles and core radii that have been determined from detailed modelling of highly-constrained cluster lenses (Kneib et al. 1995). In addition, if we fit the radial shear profiles in our clusters with the form, $\langle g_1 \rangle \propto r^\gamma$, we obtain $\gamma = -1.0 \pm 0.4$, further supporting our assumption of an isothermal mass profile. By including an inner annular cutoff our results are relatively insensitive to the mass profile of the innermost regions where strong cluster-to-cluster variations may exist. Some clusters may have shallower mass profiles, because of substructure or elliptical mass distributions, leading to our apparently underestimating their L_X for a given shear. However, it is not straightforward to determine the effect such complications would have on the X-ray properties of the clusters and so we have chosen to retain our simple description of the cluster potential.

As a baseline in comparing models of the evolution of the mass and X-ray emission in our distant clusters we have chosen to construct a null-hypothesis. We start with our analytical isothermal sphere model of the cluster potential and calculate the shear produced as a function of cluster mass, by lensing

of a field population parameterized by the same no evolution $N(z)$ used to correct the observed shear amplitudes (Smail et al. 1991). The shear is calculated for a lens placed at $z = 0.4$ and integrated within the appropriate annulus. We then determine the equivalent X-ray temperature for our cluster mass, assuming the intracluster gas is in hydrostatic equilibrium at the virial temperature of the cluster potential. We thus have a relationship between X-ray temperature and shear strength and using the locally observed X-ray temperature–bolometric luminosity relation ($T_X \propto L_X^{0.30}$, Edge & Stewart 1991; David et al. 1993) we can transform this to an L_X –shear relation for the distant clusters. To convert from bolometric luminosity to L_X in the 0.3–3.5 keV band we assume a simple bremsstrahlung spectrum for the cluster emission. A power-law fit to the final prediction using the form, $\langle g_1 \rangle = A_x L_X^{\alpha_x}$ (with L_X in units of $h^{-2} 10^{44}$ ergs sec^{-1} in the 0.3–3.5 keV band), gives $\alpha_x = 0.30 \pm 0.05$ and $A_x = 0.178_{-0.032}^{+0.039}$. This prediction, based on the local L_X – T_X relationship, is termed our “no evolution” (NE) model.

A number of more elaborate evolutionary models have been discussed in the literature (Kaiser 1991; Evrard & Henry 1991; Waxman & Miralda-Escudé 1995; Bower 1996) to explain the observed X-ray luminosity function (XLF) and its evolution. These models predict different forms for the cluster temperature–luminosity relationship and we can compare these with our null-hypothesis. The models are mostly based on analytical self-similar models for cluster evolution using the Press-Schechter formalism. We will concentrate on the family of models discussed by Bower (1996), who uses a simple parametrisation for the entropy evolution in the clusters to predict the luminosity–temperature relationship for a number of likely scenarios. With an appropriate choice of the index of the mass power spectrum, n , these models can fit the local XLF and L_X – T_X relation, although the effect of n on the evolution in the L_X –shear relation is weak and so we have chosen to adopt $n = -1.5$.

For a bolometric detector Bower predicts the following relation between the characteristic temperature and bolometric luminosity of clusters: $T_X \propto (1+z)^{3\epsilon/11} L_X^{4/11}$, where ϵ parameterises the entropy evolution. We will restrict our discussion to the the four values of ϵ discussed by Bower: $\epsilon = -3.7, -1.0, 0.0$ and 1.0 . Of these, $\epsilon = -3.7$ corresponds to the self-similar cluster evolution discussed by Kaiser (1991), where the gas evolution is entirely driven by the cluster growth. $\epsilon = -1.0$ is an intermediate case, where the compression of the gas during the cluster collapse is limited to some extent by the minimum allowed entropy set by pre-heating. $\epsilon = 0.0$ has a constant entropy in the cluster core, and $\epsilon = 1.0$ is a situation where gas cooling in the cluster core dominates the evolution. We normalise these models by fitting each to the local L_X/T_X data given by Edge & Stewart (1991) and, using the evolution of the characteristic parameters, predict the L_X -shear correlations at $z=0.4$.

The relationship between the velocity dispersion of cluster galaxies and the shear strength of the cluster

is straightforward to determine, assuming there is no velocity bias or similar effect in the cluster members. However, it should be noted that the velocity dispersions typically sample a larger region of the cluster than the the X-ray emission, which is centrally peaked and thus better matched to the aperture of our lensing mass measurements. For our sample definitions, using the form, $\langle g_1 \rangle = A_v \sigma^{\alpha_v}$ (for σ in units of 10^3 km sec^{-1}), gives $\alpha_v = 2.0$ and $A_v = 0.2$.

4. Lensing Results

In this section we now compare our cluster shear measurements with other estimates of the cluster masses. By determining the correlations between these properties and comparing these to the equivalent, locally-derived forms, we can investigate whether the physical mechanisms underpinning the local relationships remain applicable in more distant clusters.

4.1. The Strong Lensing Regime

We first undertook a visual search of the HST frames to uncover strongly-lensed features in the clusters. Such features normally occur when the mass density in the central regions of the cluster exceeds a critical value. If our clusters have similar mass profiles we would thus expect the presence of strongly-lensed features in the cluster cores to correlate with the shear strength of the clusters measured on larger scales. The results of this search are given in Table 1.

We find candidate features in 65% of our clusters, including both giant arcs and multiply-imaged pairs. The presence of strongly-lensed features was not a selection criterium for the majority of our clusters (the exceptions being A2218, Cl0440–02 and Cl0024+16) and thus their high rate of occurrence demonstrates the benefits of working at high-resolution for the identification of lensed objects. It is also interesting to note that the lensed features in 3 of the 7 strong-lensing clusters (A2218, AC118, Cl0054–27) indicate that these clusters contain multiple mass components (e.g. Fig. 1). These lensed features and the more detailed view of the cluster mass distributions they provide are dealt with in a separate article. We discuss below the correlation between the presence of strongly-lensed features and the mean cluster shear.

4.2. The Weak Lensing Regime

We now discuss our weak shear measurements in the context of $L_X-\langle g_1 \rangle$ and $\sigma-\langle g_1 \rangle$ relationships.

4.2.1. The L_X – $\langle g_1 \rangle$ Relation

Fig. 2 shows the average tangential shear, within our adopted annular region, versus the cluster’s X-ray luminosity. We detect a coherent shear field, arising from gravitational lensing by the cluster potential, in 11 of the 12 clusters in our study. Those clusters which show strongly-lensed features are indicated with filled symbols. Their distribution in Fig. 2 shows that the average tangential shear correlates well with the projected surface density in the inner ~ 50 – $100 \text{ h}^{-1} \text{ kpc}$. This would be expected if the clusters have roughly similar mass profiles. The division between those clusters capable of forming multiply-imaged features and those that cannot provides a rough mass estimate for the central regions. For a background source at $z \sim 1$, this region at $\langle g_1 \rangle \sim 0.1$, is equivalent to a mass of $M(< 50 \text{ h}^{-1} \text{ kpc}) \sim 2 \times 10^{13} \text{ h}^{-1} M_\odot$.

A correlation is also apparent between the X-ray luminosity and the mean shear, with the clusters with stronger shear fields showing higher luminosities. We fit a power-law, $\langle g_1 \rangle = A_x L_X^{\alpha_x}$, to this correlation and determine best fit parameters for the slope, α_x , and normalisation, A_x . We obtain a best fit of $\alpha_x = 0.58 \pm 0.23$ and $A_x = 0.074 \pm 0.017$. However, the likelihood contours for this fit (Fig. 3) shows that we can only realistically constrain a combination of the slope and the normalisation. The rms scatter around this correlation is roughly a factor of ~ 2 , which is not much larger than would be expected from geometrical effects if the clusters are a family of prolate ellipsoids with moderate axial ratios. A further indication that some of the observed scatter is intrinsic comes from the cluster Cl0054–27. Fig. 2 shows this cluster has a relatively low X-ray luminosity for its apparent shear amplitude. This is unlikely to be statistical scatter as the strong shear is supported by the presence of strongly-lensed features in the cluster center. We suggest that this cluster is an example of a system which is elongated along the line-of-sight, leading to a lower X-ray luminosity than expected for its high mass surface density. It should be noted that standard X-ray deprojection, which assumes spherical symmetry, applied to such a system would lead to an incorrect estimate of the cluster mass.

Fig. 2 shows the predicted upper bound relation expected in the case of a 100% shear measurement efficiency in our null-hypothesis (an unevolving L_X – T_X relationship). This line does approximately define the upper bound for the sample. The estimated efficiency from our simulations is 75% (§3) and the prediction in this case is also shown. The data agrees with this prediction at the $\sim 99\%$ confidence limit. Reducing the mean redshift of the background field population used in our model would further improve the agreement. For example, a reduction in the median redshift of the field population by 10% leads to a $\sim 10\%$ increase in the corrected shear estimates for the clusters, the effect is stronger for the more distant clusters. We conclude from Fig. 2 that there is no evidence for strong evolution of the cluster L_X –temperature relationship between $z \sim 0$ and $z \sim 0.4$.

Next we examine the family of models from Bower (1996) discussed earlier. We plot the track followed by the models as a function of ϵ on Fig. 3, marking the positions of the four cases listed above. Any values of $\epsilon \lesssim 0.5$ would provide as good a description of the data as our NE model, although lower values are preferred. The 90% confidence limits on the range of ϵ given above are $-3.7 \leq \epsilon \leq -0.3$. Very low values for ϵ , close to the self-similar case $\epsilon \sim -3.7$, are excluded by the observed evolution in the cluster XLF (Kaiser 1991; Bower 1996). From the observed evolution in the XLF and temperature function of distant clusters Bower (1996) derives limits of $-0.5 \leq \epsilon \leq 3.8$ for an $n = -1.5$ power spectrum. We can see that both the lensing and X-ray data are roughly consistent with a value in the range $\epsilon \sim -1-0$, if we include the possibility of changing the index for the mass power spectrum. This case represents mild preheating of the X-ray gas, insufficient to produce a constant entropy core at all epochs, but strong enough to significantly alter the evolution.

4.2.2. The $\sigma-\langle g_1 \rangle$ Relation

When we study the relationship between $\langle g_1 \rangle$ and velocity dispersion shown in Fig. 4 we come to a very different conclusion to that obtained for the $L_X-\langle g_1 \rangle$ relation. While the upper bound predicted by the model does lie above the observations, the same is also true when we include our best estimate of the observational efficiency, 75%, in contrast to Fig. 2 where this line passes through the data points. To achieve a similar agreement between the observations and the model predictions as that seen for the $L_X-\langle g_1 \rangle$ relation we need to decrease the predicted shear by a further 60%, equivalent to an increase in the predicted velocity dispersions of $\sim 40-70\%$.

Given the relatively good agreement seen in the $L_X-\langle g_1 \rangle$ correlation we suggest that this offset in the $\sigma-\langle g_1 \rangle$ relation most likely arises from a general and systematic over-estimation of our cluster velocity dispersions, by factors of $\sim 40\%$. This is the first time that a quantitative estimate of the bias in velocity dispersion estimates for distant clusters has been made. However, we reiterate that the velocity dispersions are typically measured over larger regions of the clusters than the other mass estimates discussed here. We might expect that the quoted discrepancy would decrease if we restricted ourselves to galaxies projected close to the cluster core, or for particular subsamples of the clusters members (e.g. the E/S0 population). The latter will be a particular concern for the spectroscopic samples from Dressler & Gunn (1992), which were specifically aimed at identifying blue cluster members, if the dynamics of such galaxies are not representative of the cluster population as a whole. Unfortunately, the velocity information available at the present time is insufficient to allow us to select the statistically reliable subsets needed to test our suggestions on a cluster-by-cluster basis. We can, however, combine the velocity information for

a number of clusters and determine how the typical dispersion would change if we restricted our sample to only the “passive” galaxies. Using the redshift and spectral information from Dressler & Gunn (1992) we find that the typical cluster dispersion for the passive population is $\sim 25\%$ less than the whole sample. Such a decrease would obviously go a long way to reconciling the observed dispersion with the lensing predictions. A related possible cause of the systematic overestimation of the velocity dispersions arises from the difficulty of identifying outliers and substructures in the distributions for individual clusters when dealing with samples of only ~ 30 members per cluster (Carlberg et al. 1996). An indication of the change in the velocity dispersion when using a more complex iterative rejection of interlopers and no color selection for the galaxies, comes from a comparison of our estimated dispersion for Cl0016+16 with that from the slightly larger sample amassed for this cluster by the CNOC collaboration (Carlberg et al. 1996). The CNOC group estimate $\sigma = 1243 \text{ km sec}^{-1}$, a value 40% lower than the value given in Table 1, in line with our estimate of the offset given above.

The extent of the overestimation of the cluster dispersions in our sample, which all have apparently well sampled distributions, and its variation with the sample definition may be also indicating that *most* distant clusters are dynamically unrelaxed, containing coalescing and unvirialised mass sub-components as well as more general in-fall (Bower et al. 1996). Direct evidence of such sub-components comes from the strongly-lensed features in the most massive clusters. In $\sim 40\%$ of these clusters, the morphologies of the strongly-lensed features indicate that the mass distributions contain multiple components on projected scales of $100\text{--}300h^{-1}$ kpc. This leads us to suggest that these massive distant clusters are observed in a period of rapid growth.

4.3. Mass to Light Ratios

We next wish to convert the shear estimates for our clusters into masses and combine these with measurements of the luminosity of the cluster population within a similar aperture to determine the mass to light ratios for the various clusters. Using a singular isothermal sphere model for the clusters and the no evolution $N(z)$, we estimate that an observed shear of $\langle g_1 \rangle = 0.1$ measured inside a $200 h^{-1}$ kpc aperture in a cluster at a redshift of $z = 0.4$ corresponds to a projected mass within the same radius of $M = 9.8 \times 10^{13} h^{-1} M_{\odot}$. We use this value along with the observed shears to give the cluster aperture masses listed in Table 2.

Weak lensing observations have been published for the cluster Cl0016+16 from ground-based observations (Smail et al. 1995a). Converting their values from a $600h^{-1}$ kpc diameter aperture to that used here we find that their lower limit to the cluster mass inside a radius of $200h^{-1}$ kpc is $M \geq 0.9 \times 10^{14} h^{-1} M_{\odot}$

and their best estimate for the mass is $M \sim 2.9 \times 10^{14} h^{-1} M_{\odot}$. This is in reasonable agreement with our value of $M \sim (1.87 \pm 0.64) \times 10^{14} h^{-1} M_{\odot}$ from Table 2, particularly given the difficulties of the ground-based observations and the large corrections which have to be applied to them.

To estimate the luminosity associated with the cluster galaxy population we must first attempt to separate and correct for the contamination by field galaxies. We have chosen to do this using the morphologically classified field counts from the HST Medium Deep Survey (MDS, Griffiths et al. 1994). By similarly classifying the galaxy populations in our cluster fields we can then correct the individual galaxy classes for field contamination to determine total luminosities for the various cluster populations. The morphological catalogs of galaxies in these clusters are given in Smail et al. (1996) and Couch et al. (1996) to a limit of $I_{814} = 23.0$ or $R_{702} = 23.5$. These samples have been visually classified onto the revised Hubble scheme, similar to that used by the MDS, in a manner described in the associated papers. We fit power laws to the differential number counts for the different morphological classes (E, S0, Sab, Scd, Irr) from the MDS catalogs and use these to subtract off the counts in the cluster fields. Having done this we then convert the magnitudes of the resulting cluster populations to M_V using the relevant K correction for the spectral energy distributions (SED) of the different morphological classes (assuming that the SED of a particular morphological type is not a function of epoch). These field-subtracted luminosity functions are binned into two samples: E and all galaxies (E-Irr), which are then integrated down to a fixed absolute magnitude ($M_V = -18.5$) and corrected for both the proportion of the population missed due to the annulus falling outside the frame (assuming all the galaxy populations follow an isothermal distribution) and the fraction of light missed from galaxies below the adopted magnitude limit (for this we use the extrapolate the fits to the cluster elliptical and spiral LFs given in Smail et al. 1996) to obtain total luminosities.

We have chosen to calculate total luminosities for the elliptical population as well as for the whole cluster population. There are three reasons for this: (1) elliptical galaxies are a large fraction of the cluster population, but only a relatively small proportion of the field population and thus the field contamination of this luminosity estimate ought to be lower than a sample comprising both ellipticals and spirals; (2) the majority of the clusters included in this study contain large populations of blue star-forming galaxies which are absent from similar environments today consequently the blue luminosity of the whole cluster population may be artificially raised; (3) the evolution of the elliptical cluster population is better understood than the clusters spirals (Ellis et al. 1996; Barger et al. 1996), this allows us to robustly predict the luminosity of the elliptical population at the current epoch.

We show the relationship between cluster aperture mass and luminosity for the various sample definitions in Fig. 5 and list the values in Table 2. For the whole cluster population, we obtain a median

mass to light ratio of $M/L_V^{\text{all}} = 180_{-80}^{+140}h(M/L_V)_\odot$, where the limits are the quartile points of the distribution. That for the ellipticals only is $M/L_V^{\text{E}} = 330_{-110}^{+210}h(M/L_V)_\odot$. Correcting for the observed evolution in the elliptical galaxy population to the individual clusters ($\delta M_V \sim -0.6$ to $z = 0.4$ c.f. Barger et al. 1996) we obtain $M/L_V^{\text{E}}(z = 0) = 620_{-240}^{+250}h(M/L_V)_\odot$. For comparison $M/L_V = 1400\text{--}1600h(M/L_V)_\odot$ is required locally for closure density (Binney & Tremaine 1987).

Clearly the most interesting of the three mass to light ratios listed above is that for the whole cluster population. To convert this to a present-day value we must first determine the luminosity evolution of the whole cluster population from $z = 0.4$ to the present day. Unfortunately, studies of the Butcher-Oemler effect in distant clusters (Couch et al. 1994; Dressler et al. 1994) show that the evolutionary history of the spiral galaxies, which comprise 25–65% of the total cluster luminosity in these systems, is likely to be complex and so we do not pursue this approach. Instead we turn to the elliptical population, whose evolution is better understood. Here, however, we are only dealing with a proportion of the total cluster luminosity and so we will only be able to derive an upper limit for the cluster M/L at the present epoch. Including the fading of this population between the observed epoch and the present day and assuming that this mass to light ratio is representative of the global value we have $\Omega_0 \leq 0.4 \pm 0.2$.

Looking at the scatter in the various measurements we note that the luminosity of the elliptical population is better correlated with the cluster aperture mass than the luminosity of the whole cluster population. Moreover, the relative scatter for the M/L^{E} is only $\sim 40\%$, very similar to the median error in the cluster masses from the lensing analysis. This similarity leaves open the possibility that in the majority of the clusters all the observed scatter in the M/L^{E} arises from measurement errors and hence that the cluster M/L^{E} ratio is a constant. Such a conclusion would obviously have profound implications for the formation mechanism of cluster ellipticals. However, we also note that some clusters in Fig. 5 populate a tail to considerably higher M/L's. These clusters tend to be more massive than the mean in our sample, and some variation in cluster property (e.g. mass profile) with mass may therefore be driving their anomalous M/L's.

Finally, we give an illustration of the unique insights which gravitational lensing provides into the structure and evolution of clusters. In Fig. 6 we plot the spiral fractions of the clusters from Table 2 (f_{sp}) against their aperture masses. This figure exhibits a transition between the spiral fractions of low and high mass clusters, the change over apparently occurring at a mass of $M \sim 2 \times 10^{14}h^{-1}M_\odot$. Above this mass the central regions of the clusters ($\leq 0.5h^{-1}$ Mpc) are relatively devoid of spiral galaxies. This figure bears a striking resemblance to Fig. 16 of Allington-Smith et al. (1993), where they plot blue fraction, f_B , versus richness for local groups and clusters. Allington-Smith et al. found a sharp decrease in the

blue-fraction for the richest systems (with total luminosities above $L_V \sim 3 \times 10^{12} h^{-2} L_\odot$, Oemler (1992)). However, when they constructed a similar plot for distant groups and clusters (their Fig. 19) they saw little evidence for a similar decrease in f_B with increasing richness. The existence of a sharp discontinuity in our morphology-environment relation (when determined from f_{sp} and cluster mass) maybe indicating their use of total richness as an indication of system mass undermined their analysis. Clearly more data is required to investigate the feature in the morphology-environment relation, and to untangle it from the strong redshift evolution observed in the relation (Fig. 6, Couch et al. 1994; Dressler et al. 1994). Nevertheless, we stress that the impact of adding lensing masses to the list of observable characteristics of distant clusters may be felt across a wide range of research fields.

5. Conclusions

Our study represents the first analysis of the weak gravitational lensing signal in a large and diverse sample of distant clusters. The major advantage of our study has been the use of HST to detect the weak shear, where we gain over ground-based telescopes by the high efficiency for recovering the true shear.

Summarising the main conclusions of our survey:

- We have measured a tangential alignment of the images of faint background galaxies in 11 out of a sample of 12 distant clusters imaged with HST. The high detection rate demonstrates the power of high-resolution imaging in this type of study.
- We show that the presence of strongly-lensed features within the cores of a large fraction of our clusters correlates well with the shear signal measured on larger scales from the more weakly distorted arclets.
- We find a reasonable correlation between the X-ray luminosities of our clusters and their masses, as estimated from the gravitational shear fields in the central $\sim 0.5 h^{-1}$ Mpc of each cluster. The scatter about this relation is only a factor of two – not much larger than that expected from projection effects in a family of randomly oriented ellipsoidal clusters.
- We compare the L_X –shear data with a prediction made on the basis of the local L_X – T_X relation and isothermal mass and gas distributions in the clusters. We find that the local relation is an adequate description of the distant cluster sample, after allowance has been made for a number of observational effects and uncertainties. We thus conclude that there is no strong evidence for evolution in the L_X – T_X relationship since $z \sim 0.4$.
- The observed evolution in the L_X – T_X relation can be reproduced by models introducing a modest initial

entropy into the gas prior to cluster formation, possibly resulting from pre-heating by AGN or galactic winds. Such a family of models has also been discussed in regard to the evolution of the XLF (Castander et al. 1995; Bower 1996).

- The velocity dispersions for those clusters with adequate data show that the typical cluster has a higher measured dispersion than expected on the basis of both their weak lensing and X-ray luminosities. We suggest that this arises from an inability to identify outliers and unvirialised substructures within the clusters in the relatively modest spectroscopic samples. By restricting our sample to only the passive, red populations in the clusters we can reduce these problems, and we illustrate that dispersions are reduced by a sizeable factor. Nevertheless, the strength and ubiquity of these biases raises doubts over the usefulness of virial analysis of distant clusters, when restricted to only modest samples of members.
- We convert our shear measurements into estimates of the mass in the central regions of the clusters. We then combine these with measurements of the luminosities of various samples of cluster galaxies to determine mass to light ratios for the cluster. By concentrating on the well understood elliptical population we are able to derive a limit of $M/L_V \leq 620_{-240}^{+250} h(M/L_V)_\odot$ for the clusters at $z = 0$, equivalent to $\Omega_0 \leq 0.4$.
- We illustrate the possible impact of observations such as these on studies of distant clusters by showing the correlation between the spiral fractions and the cluster masses. This shows that the morphological mix in the clusters undergoes a rapid change for clusters with masses above $M \sim 2 \times 10^{14} h^{-1} M_\odot$.

Studies such as the one presented here will be enlarged in the future through high-resolution imaging of larger samples. These should include a better-defined subset of massive distant clusters to investigate the intrinsic scatter in their X-ray/lensing properties arising from geometrical effects, as well as quantify the rate of occurrence of substructure and hence their rate of growth. An extended study would also benefit from the inclusion of more low mass systems to constrain the slope of the L_X –mass relationship at moderate redshift, as well as the morphology-mass relationship which underlies the Butcher-Oemler effect. Extending the analyzes to higher redshift will provide new constraints on the form of any evolution in the L_X –mass relation. This paper has demonstrated that weak lensing with HST provides a new and highly promising means for measuring the evolution of large scale systems in the universe.

Acknowledgements

We wish to thank Ray Lucas at STScI for his enthusiastic help which enabled the efficient gathering of these HST observations. We especially thank the anonymous referee for their constructive comments and suggestions which helped to significantly improve and clarify this paper. We also thank Richard Bower,

Alastair Edge, Vincent Eke, Jean-Paul Kneib, Jordi Miralda-Escudé and John Mulchaey for many useful conversations and assistance. IRS acknowledges support from a Carnegie Fellowship and RSE and RMS acknowledge support from the Particle Physics and Astronomy Research Council. WJC acknowledges support from the Australian Department of Industry, Science and Technology, the Australian Research Council and Sun Microsystems.

REFERENCES

- Allington-Smith, J.R., Ellis, R.S., Zirbel, E.L. & Oemler, A., 1993, *ApJ*, 404, 521.
- Barger, A.J., Aragon-Salamnaca, A., Smail, I., Ellis, R.S., Couch, W.J., Dressler, A., Oemler, A., Butcher, H. & Sharples, R.M., 1996, in prep.
- Bertin E. & Arnouts, S., 1996, *A&A*, 117, 393.
- Binney, J. & Tremaine, S., 1987, *Galactic Dynamics*, Princeton Univ. Press, Princeton, NJ.
- Bower, R.G., Bohringer, H., Briel, U.G., Ellis, R.S., Castander, F.J. & Couch, W.J., 1994, *MNRAS*, 268, 345.
- Bower, R.G., Castander, F.J., Couch, W.J., Ellis, R.S. & Bohringer, H., 1996, *MNRAS*, submitted.
- Bower, R.G., 1996, *MNRAS*, submitted.
- Carlberg, R.G., Yee, H.K.C., Ellingson, E., Abraham, R., Gravel, P., Morris, S. & Pritchett, C.J., *ApJ*, 462, 32.
- Castander, F.J., Ellis, R.S., Frenk, C.S., Dressler, A. & Gunn, J.E., 1994, *ApJ*, 424, L79.
- Castander, F.J., Bower, R.G., Ellis, R.S., Aragón-Salamanca, A., Mason, K.O., Hasinger, G., McMahon, R.G., Carrera, F.J., Mittaz, J.P.D., Pérez-Fournon, I. & Lehto, H.J., 1995, *Nature*, 377, 39.
- Couch, W.J. & Sharples, R.M., 1987, *MNRAS*, 229, 423.
- Couch, W.J., Ellis, R.S., Malin, D.F. & Maclaren, I., 1991, *MNRAS*, 249, 606.
- Couch, W.J., Ellis, R.S., Sharples, R.M. & Smail, I., 1994, *ApJ*, 430, 121.
- Couch, W.J., et al., 1996, in prep.
- Danese, L., de Zotti, G. & Tullio, G., 1980, *A&A*, 82, 322.
- David, L.P., Arnaud, K.A., Forman, W. & Jones, C., 1990, *ApJ*, 356, p32.
- David, L.P., Slyz, A., Jones, C., Forman, W., Vrtilik, S.D. & Arnaud, K.A., 1993, *ApJ*, 412, 479.
- Dressler, A. & Gunn, J.E., 1992, *ApJS*, 78, 1.
- Dressler, A., Oemler, A., Butcher, H. & Gunn, J.E., 1994, *ApJ*, 430, 107.
- Edge, A.C., Stewart, G.C., Fabian, A.C. & Arnaud, K., 1990, *MNRAS*, 245, 559.
- Edge, A.C. & Stewart, G.C., 1991, *MNRAS*, 252, 428.
- Ellis, R.S., Smail, I., Dressler, A., Couch, W.J., Oemler, A., Butcher, H. & Sharples, R.M., 1996, *ApJ*, submitted.

- Evrard, A.E. & Henry, J.P., 1991, *ApJ*, 383, 95.
- Griffiths, R.E., Casertano, S., Ratnatunga, K.U., Neuschaefer, L.W., Ellis, R.S., Gilmore, G.F., Glazebrook, K. Santiago, B., Huchra, J.P., et al., 1994, *ApJ*, 435, L19.
- Gunn, J.E., Hoessel, J.G. & Oke, J.B., 1986, *ApJ*, 306, 30.
- Henry, J.P., Soltan, A., Briel, U. & Gunn, J.E., 1982, *ApJ*, 262, 1.
- Henry, J.P., Gioia, I.M., Maccacaro, T., Morris, S.L., Stocke, J.T. & Wolter, A., 1992, *ApJ*, 386, 408.
- Holtzman, J.A., Burrows, C.J., Casterno, S., Hester, J.J., Trauger, J.T., Watson, A.M. & Worthey, G., 1995, *PASP*, 107, 1065.
- Kaiser, N., 1991, *ApJ*, 383, 104.
- Kaiser, N., Squires, G. & Broadhurst, T.J., 1995, *ApJ*, 449, 460.
- Kneib, J.-P., Ellis, R.S., Smail, I., Couch, W.J. & Sharples, R.M., 1995, *ApJ*, in press.
- Le Borgne, J.-F., Pelló, R. & Sanahuja, B., 1992, *A&AS*, 95, 87.
- Oemler, A., in *Cluster and Superclusters of Galaxies*, p29, ed. Fabian, A.C., Kluwer.
- Postman, M., Lubin, L.M., Gunn, J.E., Oke, J.B., Schneider, D.P., Hoessel, J.G. & Christensen, J.A., 1996, *AJ*, 111, 615.
- Smail, I., Ellis, R.S., Fitchett, M.J., Nørgaard-Nielsen, H.U., Hansen, L. & Jørgensen, H.E., 1991, *MNRAS*, 252, 19.
- Smail, I., Ellis, R.S., Fitchett, M.J. & Edge, A.C., 1995a, *MNRAS*, 273, 277.
- Smail, I., Hogg, D.W., Yan, L. & Cohen, J.L., 1995, *ApJL*, 449, L105.
- Smail, I., Dressler, A., Couch, W.J., Ellis, R.S., Oemler, A., Butcher, H. & Sharples, R.M., 1996, *ApJ*, submitted.
- Wang, Q.D. & Stocke, J.T., 1993, *ApJ*, 408, 71.
- Waxman, E. & Miralda-Escudé, J., 1995, *ApJ*, 451, 451.
- White, R.E. 1991, *ApJ*, 367, 69.
- Wilson, G., Cole, S. & Frenk, C.S., 1996, *MNRAS*, 280, 199.

Tables

Table 1 The cluster sample used in our analysis, including field identification, cluster redshift, filter passband, total exposure time, X-ray luminosity in the 0.3–3.5 KeV band, velocity dispersion (where known), angular scale, surface brightness limit (the 1σ fluctuation in the sky flux in a 1 sq. arcsec aperture) and whether candidate strongly-lensed features are present.

Table 2 Properties of the cluster galaxy populations. These are quoted as values corrected to an aperture of $400h^{-1}$ kpc diameter. We give the estimated cluster mass from the lensing analysis, the integrated luminosity of the elliptical population, integrated luminosity of the whole cluster population, integrated luminosity of the elliptical population evolved to the present day and the equivalent mass to light ratios. These are all corrected for luminosity in galaxies lying below the magnitude limits of the morphological samples and for those regions of the aperture falling off the frame. The final column gives the spiral fractions in the clusters, as a proportion of the whole population brighter than $M_V = -18.5$. We omit those clusters without morphologically typed samples or which are undetected in our shear measurements. The luminosities have not been corrected for reddening.

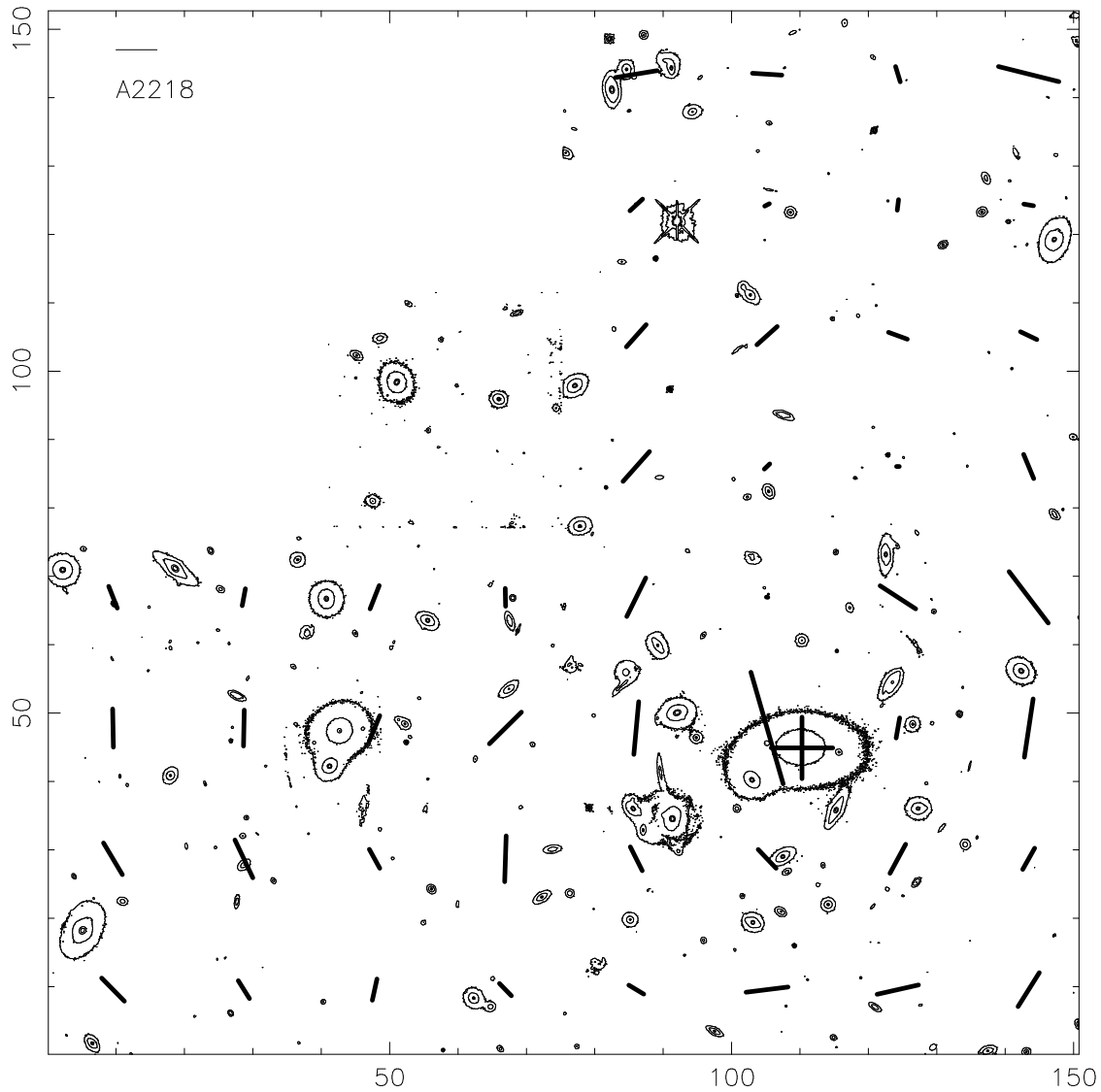


Figure 1. The shear fields, indicated by the vectors, for four of the stronger lenses in the sample. The clusters illustrated span a wide range in redshift and the shear fields show strong coherence around the lens center, which always coincides with the brightest member (marked by +). The vectors represent independent data points, each containing roughly ~ 10 faint galaxies. A perturbation in the shear field associated with a bright D galaxy just off the top-right of the frame is visible in Fig. 1(b). The scale is arcseconds and the vector at the top-left of each frame represent a 20% shear. (a) A2218 $z = 0.17$, (b) AC118 $z = 0.31$, (c) 3C295 $z = 0.46$ and (d) C10016+16 $z = 0.55$.

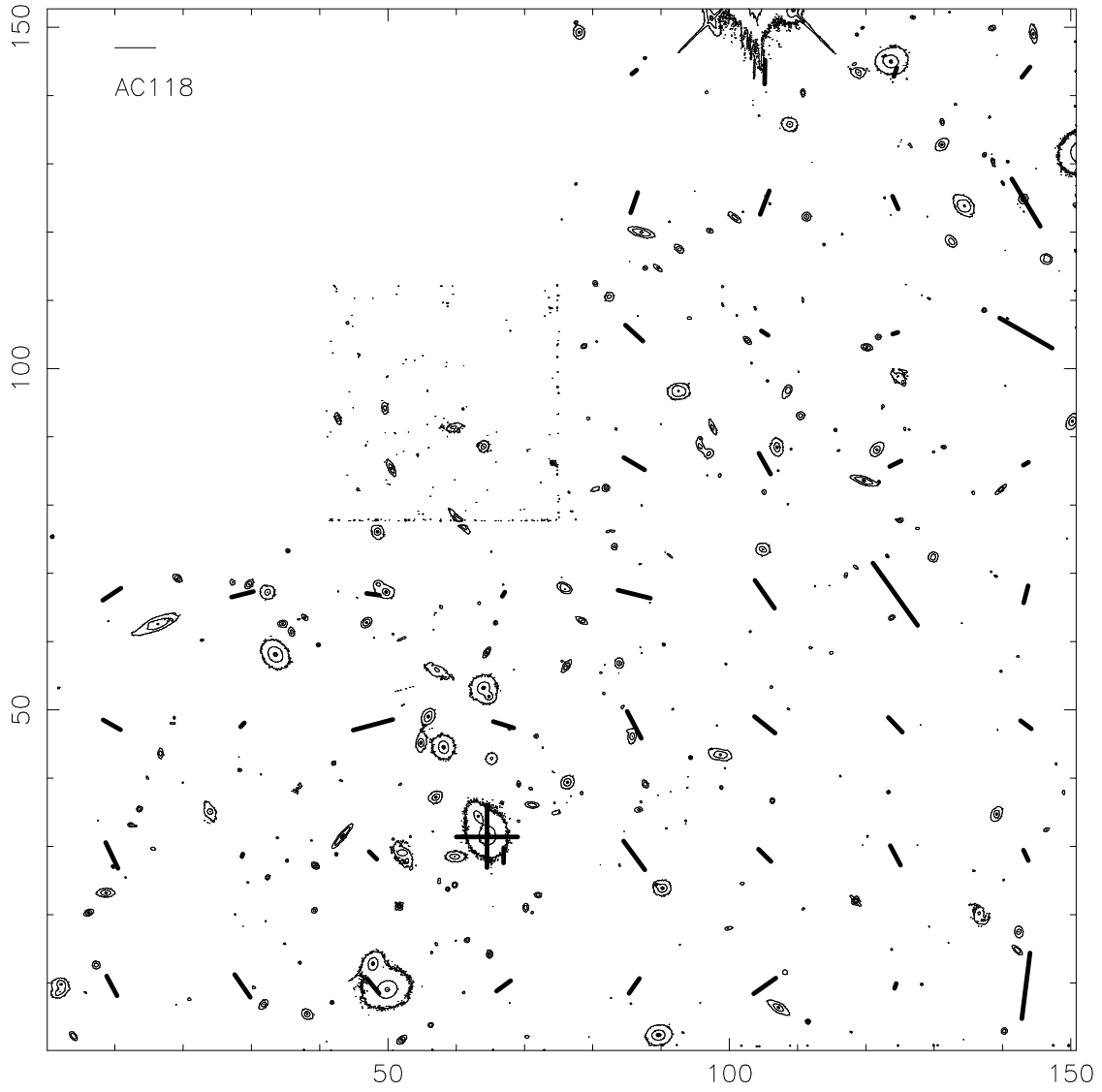


Figure 1b

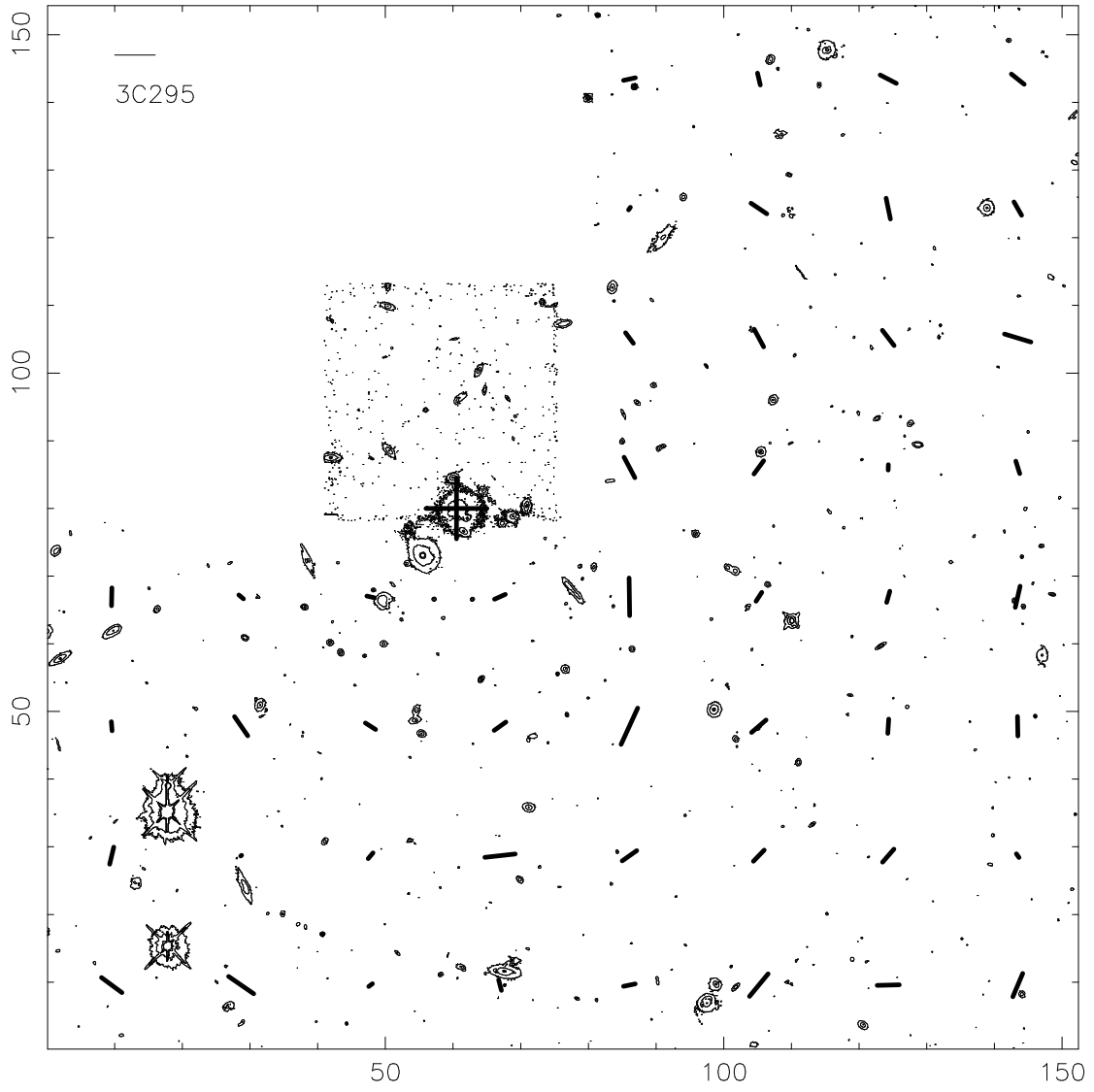


Figure 1c

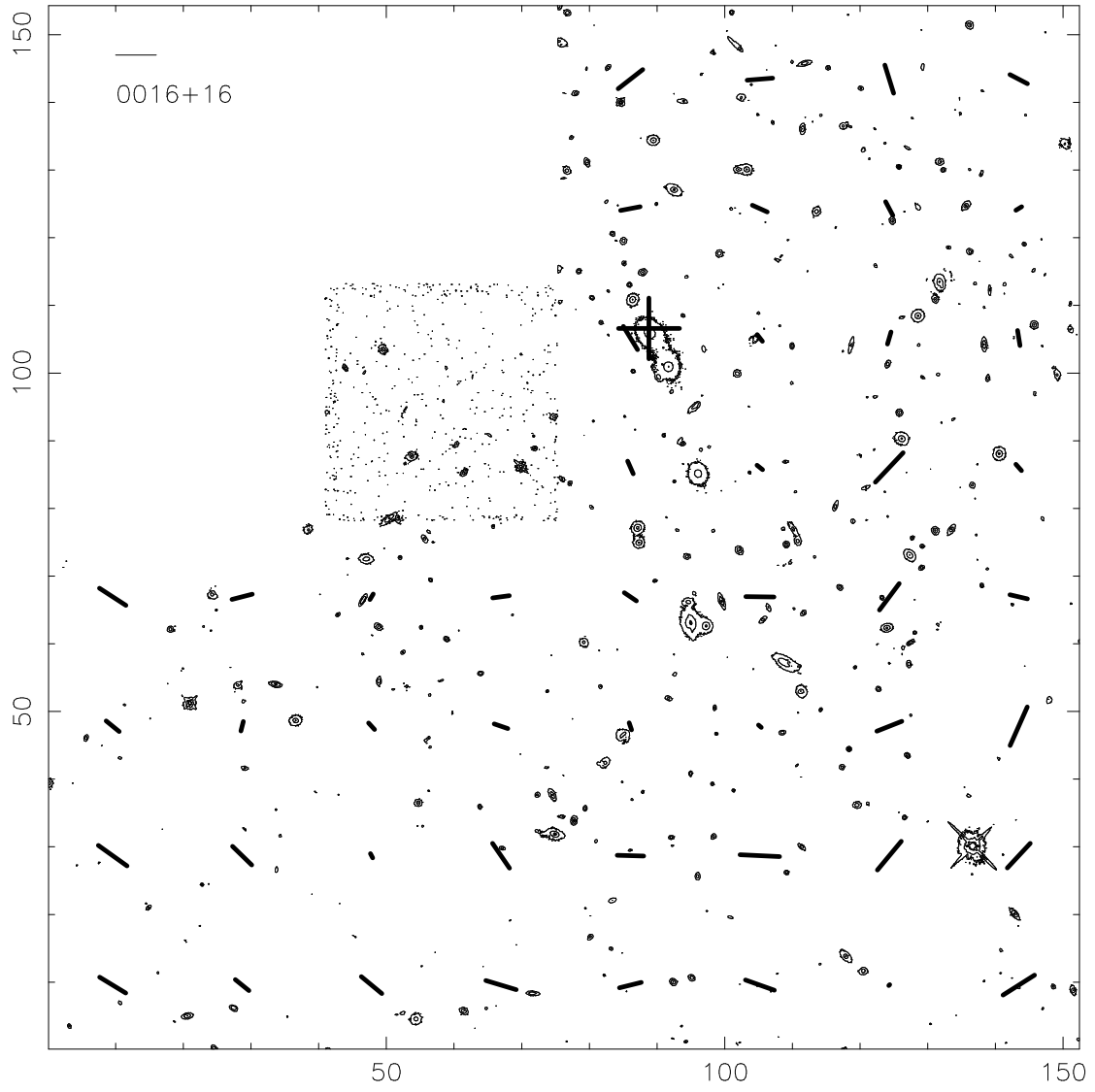


Figure 1d

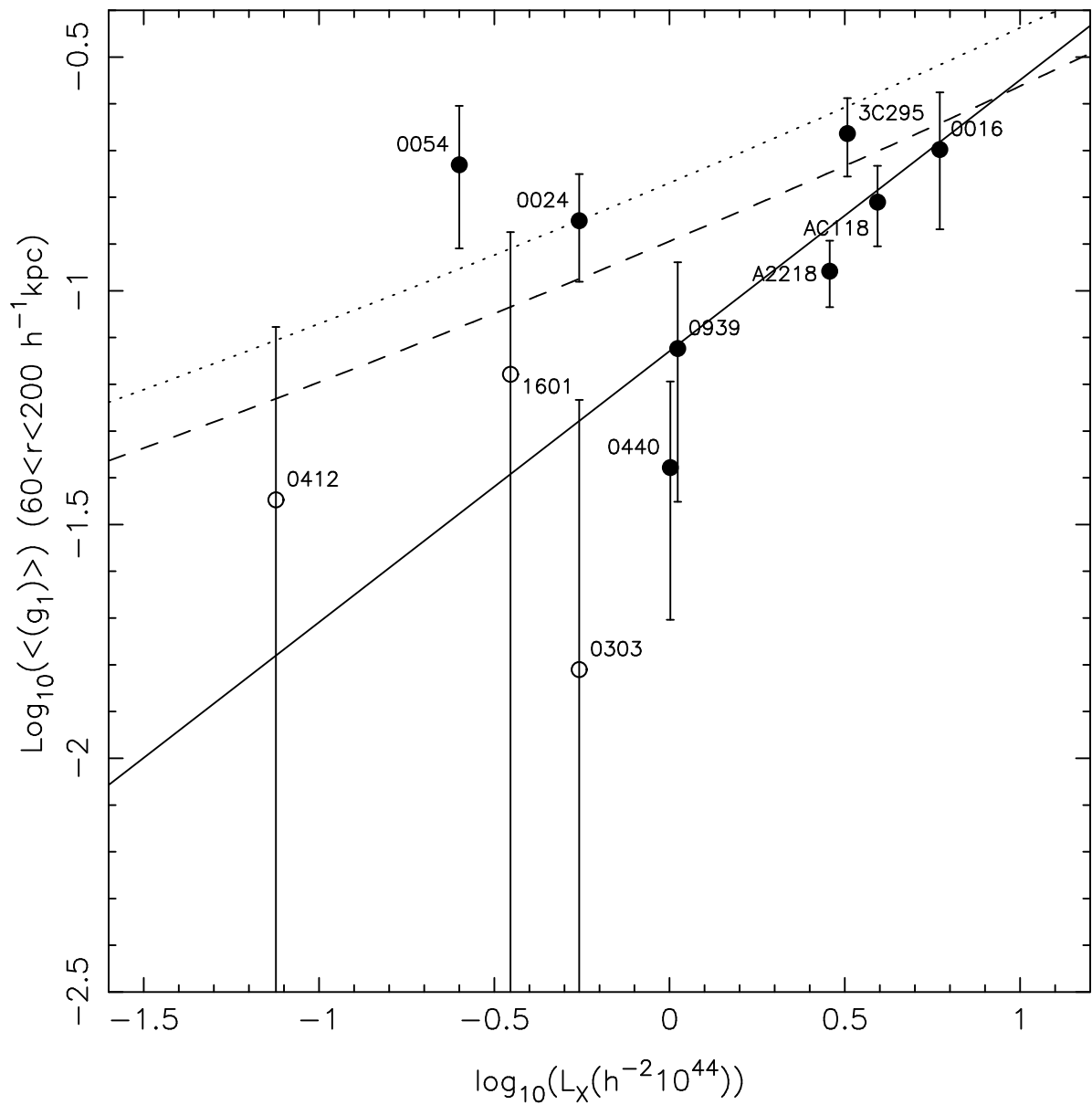


Figure 2. The correlation between the cluster X-ray luminosity and the mean shear strength, $\langle g_1 \rangle$. The error bars are 1σ boot-strap estimates and the solid line shows the best fit relationship for the data. The dotted line indicates the upper limit expected, assuming 100% measurement efficiency, in the case of our simple “no evolution” model. The dashed line represents a 75% efficiency. Filled symbols denotes those clusters which have candidate strongly-lensed features.

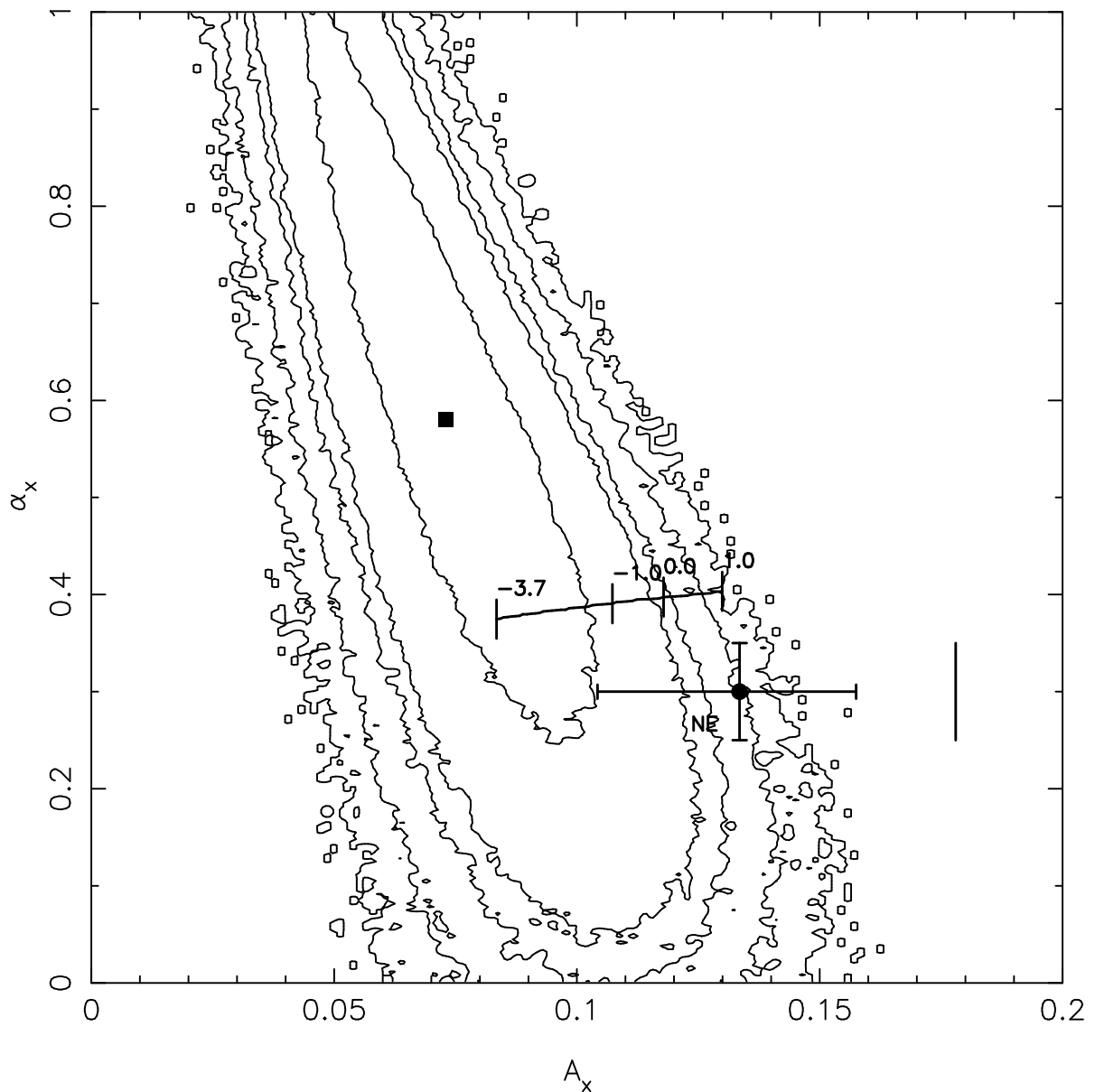


Figure 3. The best fitting parameters for a power-law description of the $L_X - \langle g_1 \rangle$ correlation, the contours are 50%, 90%, 95%, 99% and 99.9% confidence limits. The vertical bar shows the limit on the normalisation from the “no evolution” model, determined by assuming 100% measurement efficiency in our shear estimation. All observational effects will tend to drive down the predicted shear amplitude, pushing the prediction further to the left of this line. The point with error bars indicates the NE prediction assuming our best estimate of 75% measurement efficiency. The predictions of the other models discussed in the text as a function of the parameter ϵ lie along the track plotted. The points for $\epsilon = -3.7, -1.0, 0.0$ and 1.0 are marked, these all include a 75% signal degradation.

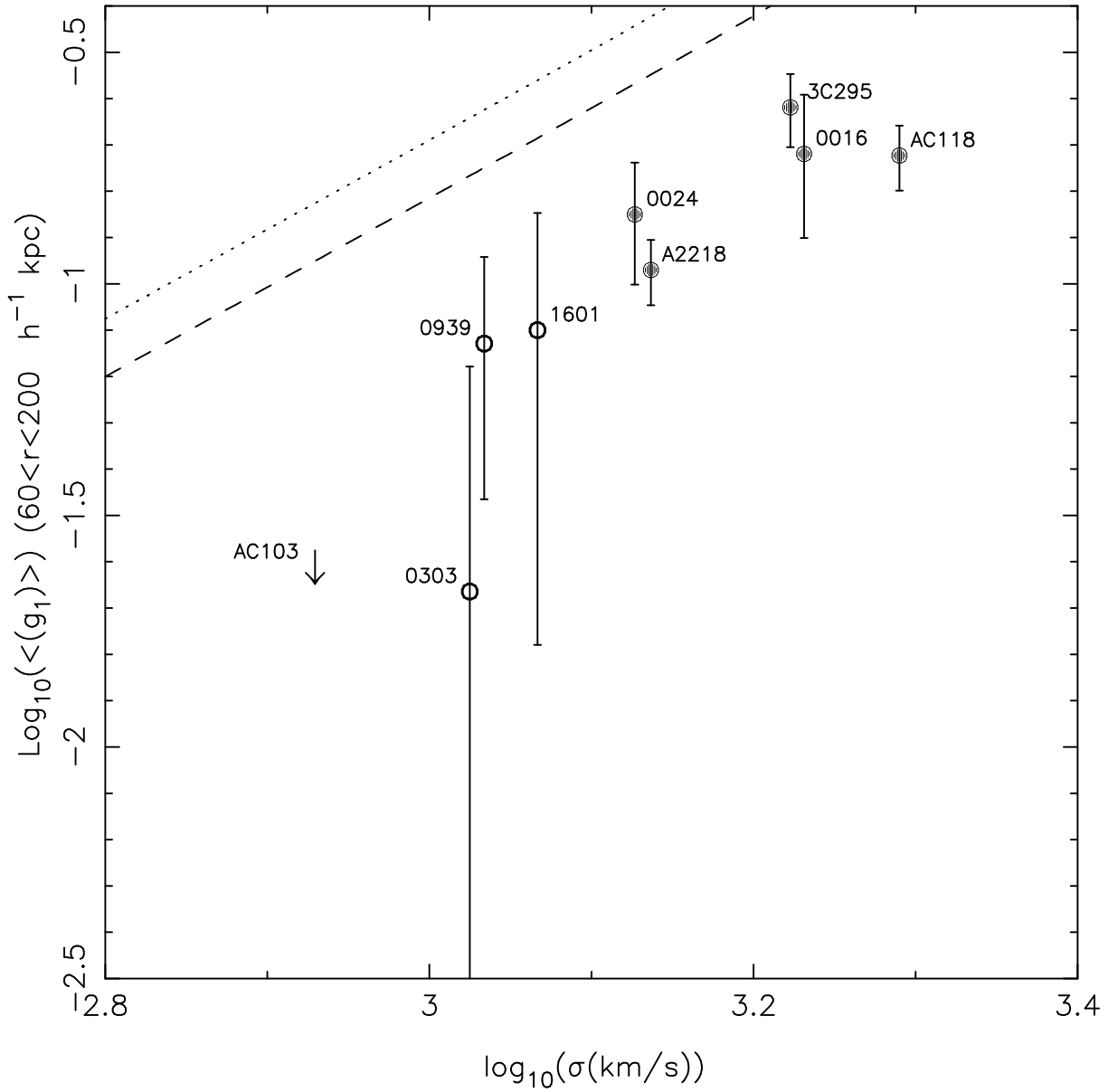


Figure 4. Correlation between cluster velocity dispersion and $\langle g_1 \rangle$ for those clusters with redshifts for at > 20 members. Error bars are 1σ . The dotted line shows the theoretical prediction assuming 100% measurement efficiency; the dashed line represents an efficiency of 75% as expected from simulations. Filled symbols denote those clusters with candidate strongly-lensed features. The arrow marks the 1σ upper limit on the AC103 shear measurement.

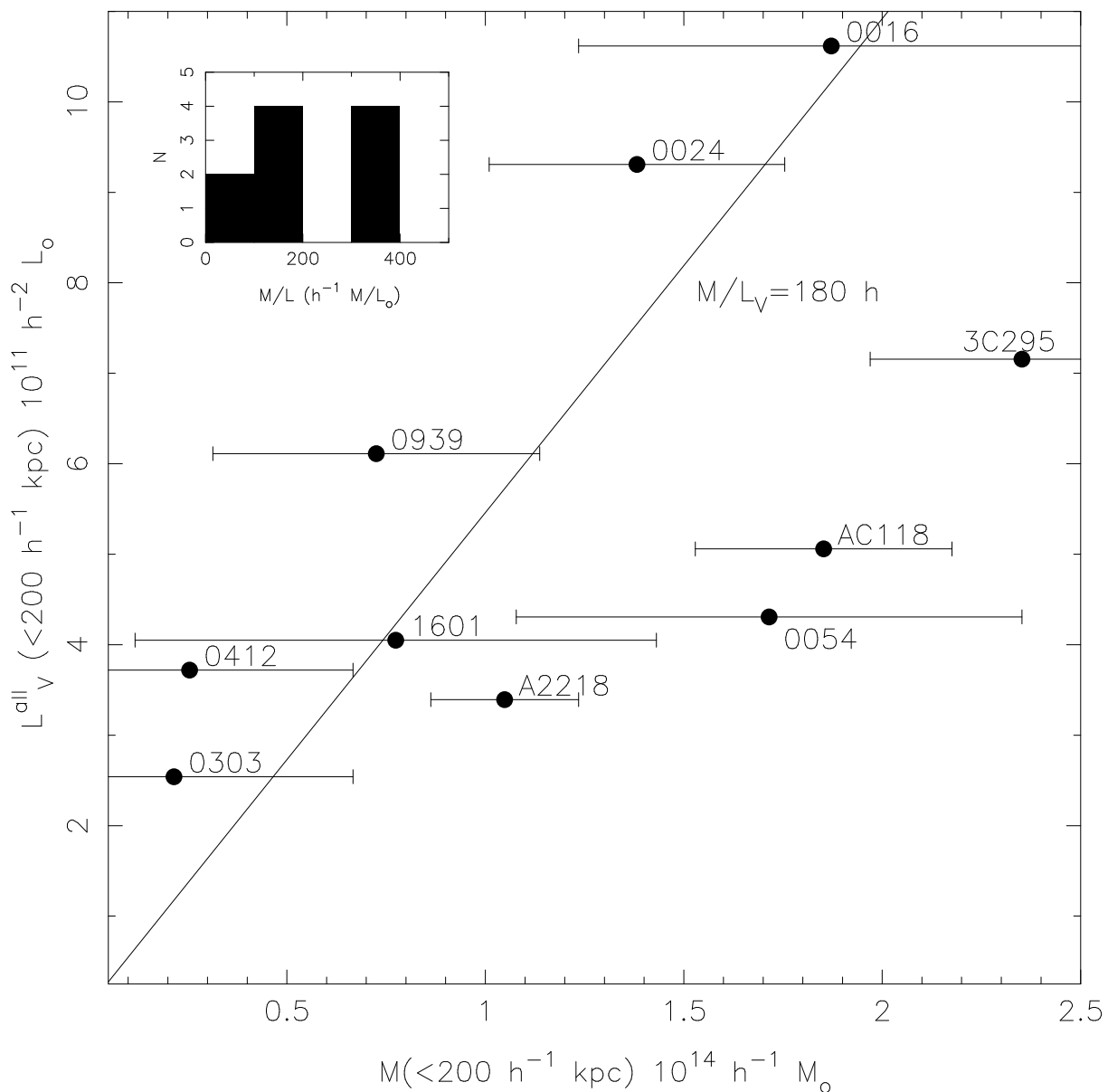


Figure 5. Plots of the total cluster mass versus integrated light in various cluster galaxy populations (both corrected to a $400h^{-1}$ kpc diameter aperture. These are shown for: (a) the whole cluster population, (b) just those galaxies classed as elliptical on the basis of their morphology, (c) the elliptical population evolved to the present day. All of the cluster luminosities have been corrected for field contamination, losses from regions of the aperture falling outside the frame and galaxies missed owing to the adopted magnitude limits as is described in the text. The solid lines show the median mass to light ratio of each sample. The histograms in each panel show the distribution of the mass to light ratios.

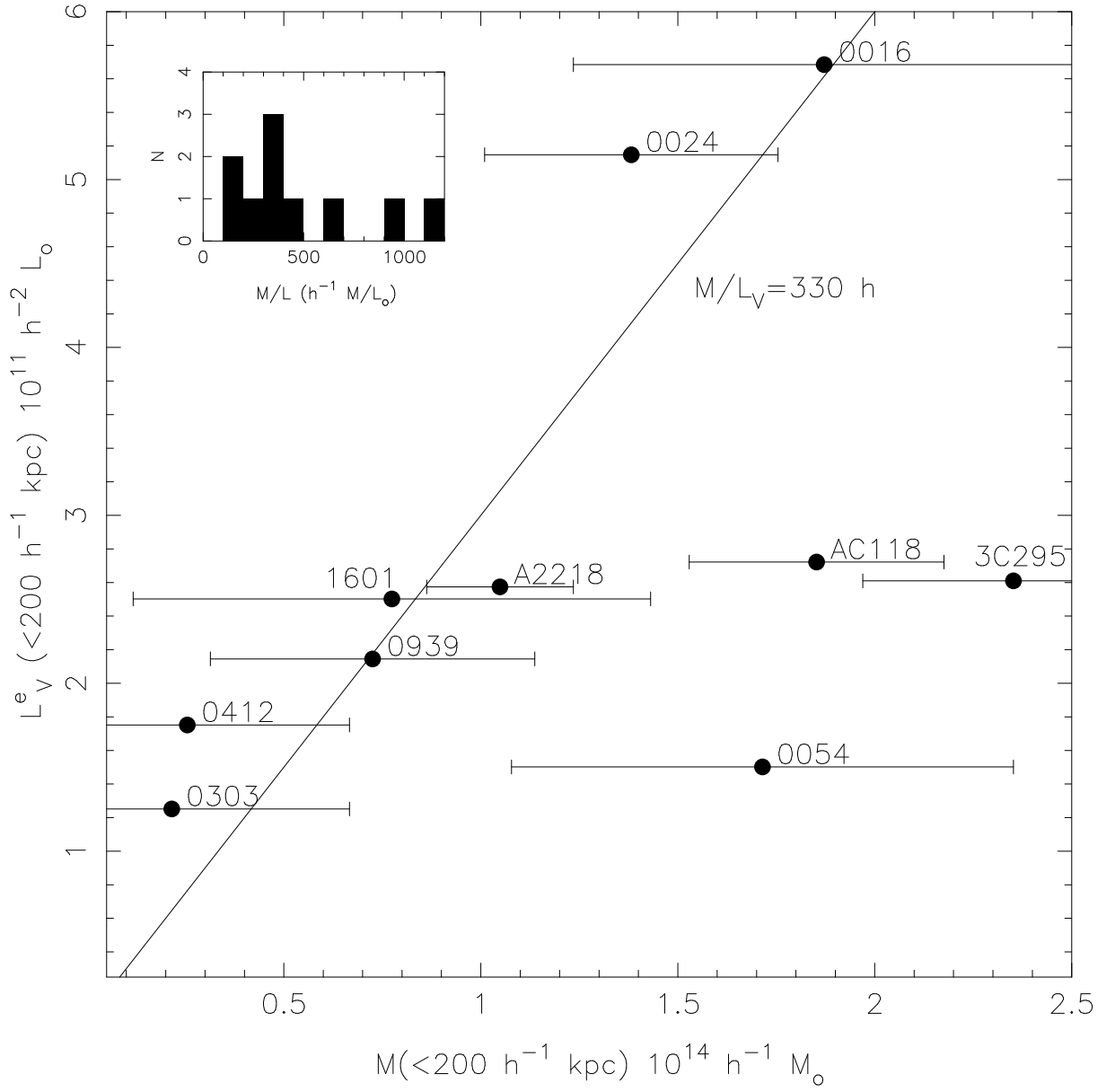


Figure 5b

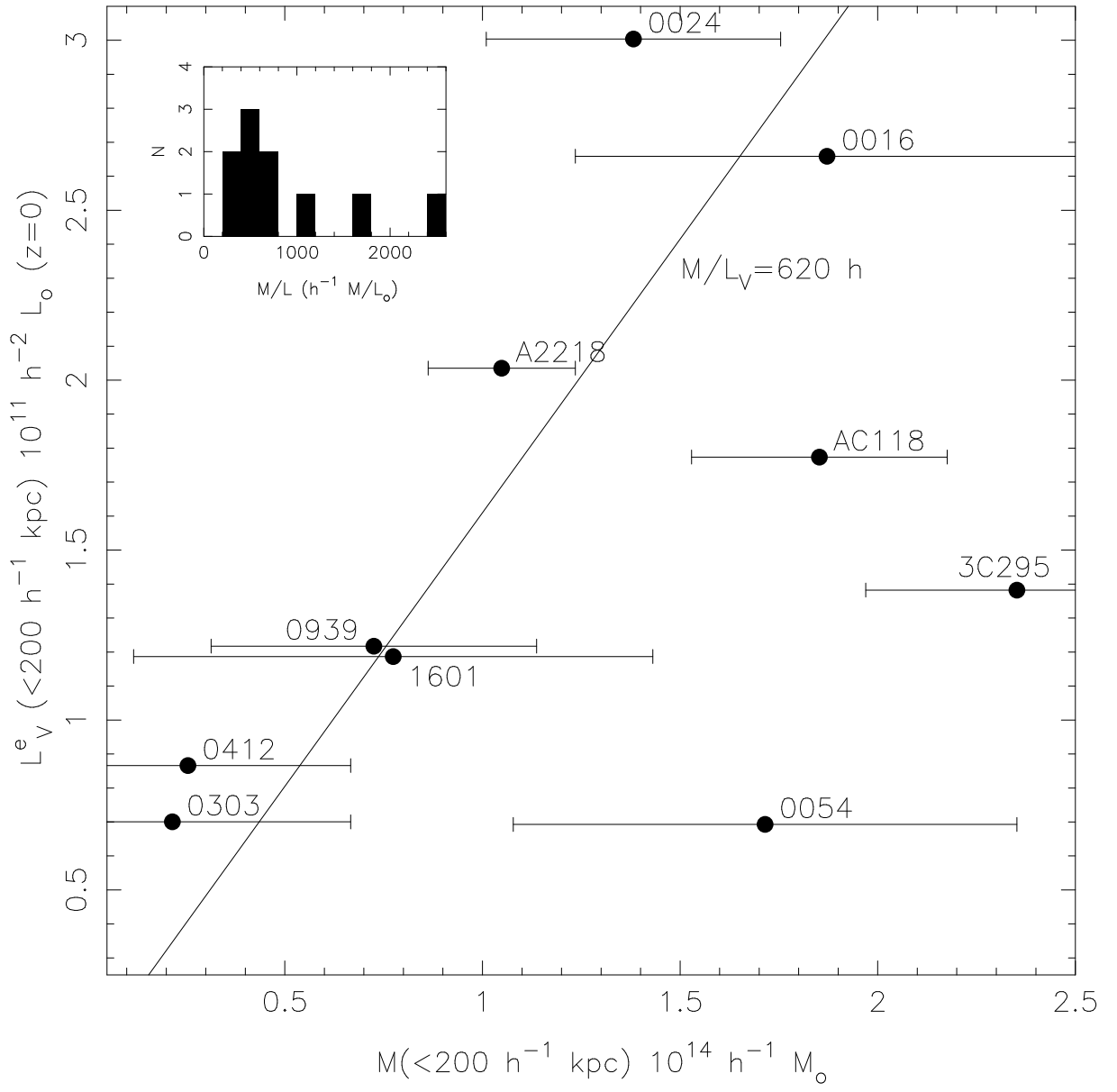


Figure 5c

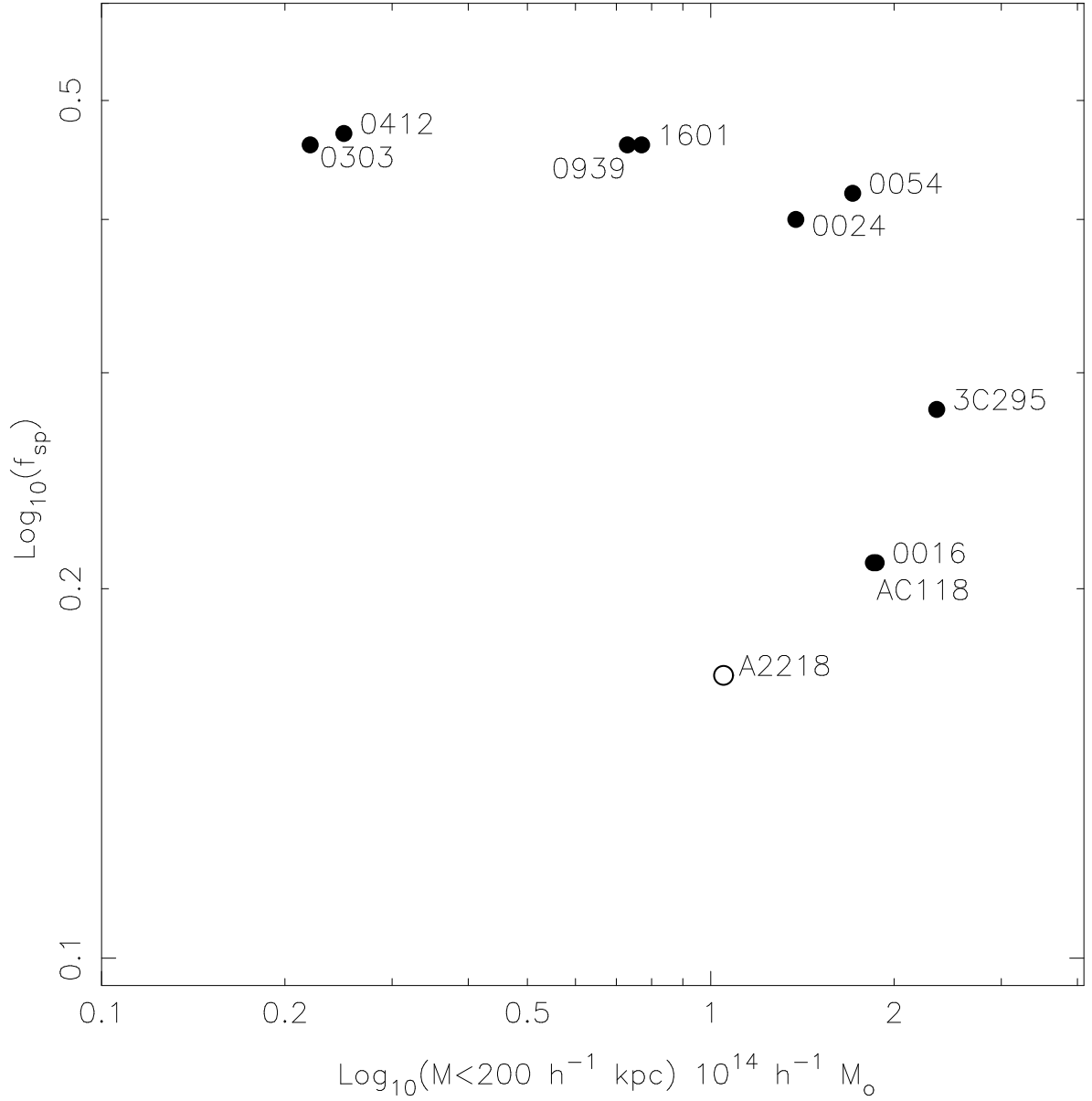


Figure 6. The number fraction of the cluster population (f_{sp}) brighter than $M_V = -18.5$ which have spiral morphology (Sab-Irr), plotted against the lensing estimate of the cluster aperture mass. There appears to be a sharp transition in the spiral fraction of the clusters at masses around $M \sim 2 \times 10^{14} h^{-1} M_{\odot}$. However, we caution that owing to the strong redshift evolution known to exist in f_{sp} (c.f. Couch et al. 1994; Dressler et al. 1994) this figure is not simple to interpret. The position of the $z = 0.17$ cluster A2218 in this figure probably reflects redshift evolution, rather than a real difference.

Table 1

Cluster	z	T_{exp}			L_X (0.3–3.5) $h^{-2} 10^{44}$	σ km sec $^{-1}$ [N]	kpc $'''$ h^{-1}	$\mu(1\sigma)$ mag/arcsec 2	Strong Lensing
		F555W	F702W	F814W					
A2218	0.17	—	6.5	—	2.85	1370 [50]	1.88	27.2	yes
Cl0440–02	0.19	—	18.4	—	1.00	—	2.03	27.1	yes
AC118	0.31	—	6.5	—	3.90	1950 [34]	2.80	27.2	yes
AC103	0.31	—	6.5	—	—	850 [29]	2.80	27.2	no
Cl0024+16	0.39	—	—	13.2	0.55	1339 [33]	3.17	27.5	yes
Cl0939+47	0.41	—	21.0	—	1.05	1081 [31]	3.26	27.3	yes
Cl0303+17	0.42	—	12.6	—	0.55	1079 [21]	3.29	27.9	no
3C295	0.46	—	12.6	—	3.20	1670 [21]	3.43	27.1	yes
Cl0412–65	0.51	12.6	—	14.7	0.08	—	3.59	27.5	no
Cl1601+43	0.54	—	16.8	—	0.35	1166 [27]	3.67	28.3	no
Cl0016+16	0.55	12.6	—	16.8	5.88	1703 [30]	3.67	26.7	yes
Cl0054–27	0.56	12.6	—	16.8	0.25	—	3.76	27.4	yes

Table 2

Cluster	M	L_V^E	L_V^{all}	$L_V^E(z=0)$	M/L_V^E	M/L_V^{all}	$M/L_V^E(z=0)$	f_{sp}
	$10^{14} h^{-1} M_\odot$	$10^{11} h^{-2} L_\odot$	$10^{11} h^{-2} L_\odot$	$10^{11} h^{-2} L_\odot$	$h (M/L)_\odot$	$h (M/L)_\odot$	$h (M/L)_\odot$	
A2218	1.05 ± 0.19	2.57	3.39	2.04	410	310	520	0.17
AC118	1.85 ± 0.32	2.72	5.06	1.77	680	370	1040	0.21
Cl0024+16	1.38 ± 0.37	5.15	9.31	3.00	270	150	460	0.40
Cl0939+47	0.73 ± 0.41	2.15	6.11	1.22	340	120	600	0.46
Cl0303+17	0.22 ± 0.45	1.25	2.54	0.70	170	80	310	0.46
3C295	2.35 ± 0.38	2.61	7.16	1.38	900	330	1700	0.28
Cl0412–65	0.25 ± 0.41	1.75	3.72	0.87	150	70	290	0.47
Cl1601+43	0.77 ± 0.66	2.50	4.05	1.19	440	190	650	0.46
Cl0016+16	1.87 ± 0.64	5.68	10.62	2.66	330	180	700	0.21
Cl0054–27	1.71 ± 0.64	1.50	4.31	0.69	1140	400	2480	0.42